Covalent vs Electrostatic Interactions in Rare Earth Systems: A Comparative Study of U(III), U(IV), and U(V) and Nd(III) Bonding Properties by DFT and CAS-PT2 Approaches†

Valentina Vetere,*,‡,§ Pascale Maldivi,‡ Björn O. Roos,|| and Carlo Adamo⊥

Laboratoire de Chimie et Physique Quantique-UMR5626, Université de Toulouse, 118 route de Narbonne, F-31062 Toulouse Cedex, France, CEA, INAC, SCIB, Laboratoire de Reconnaissance Ionique et Chimie de Coordination, 17 Rue des Martyrs, F-38054 Grenoble Cedex 9, France, and UJF, LCIB (UMR_E 3 CEA-UJF), F-38041 Grenoble Cedex 9, France, Department of Theoretical Chemistry, Chemical Center, University of Lund, POB 124, S-221 00 Lund, Sweden, and Laboratoire d'Electrochimie, Chimie des Interfaces et Modélisation pour l'Energie, UMR 7575, Ecole Nationale Supérieure de Chimie de Paris - Chimie ParisTech, 11 rue P. et M. Curie, 75 231 Paris Cedex 5, France

Received: May 26, 2009; Revised Manuscript Received: September 24, 2009

A description of the electronic structure of F_3UCO, F_3NdCO, F_4UCO, and F_5UCO has been obtained by Complete Active Space second-order perturbation theory CASPT2 calculations using a relativistic effective core potential. These multiconfigurational calculations have been compared to the DFT description combined with a quasi-relativistic ZORA scalar approach. Geometries have been optimized for both levels of calculations and frequencies computed in the DFT formalism. The bonding properties of U(III) have been compared to those of Nd(III) and of higher oxidation states of U(IV,V). Both methodologies are consistent and show a decrease of the covalent character of the U−CO bonding with a higher oxidation state, U(IV) or U(V), as well as its absence for for the isoelectronic Nd(III) species.

1. Introduction

The understanding of factors governing metal−ligand interaction in heavy element complexes is a challenging and fascinating field of research. The growing interest in the molecular properties of such systems is mostly due to their importance in various fields such as chemical processes involved in the nuclear industry, environmental aspects, catalysis, or biological applications.[1−6] In particular, in recent times, much efforts have been devoted to the understanding of the chemical causes that can differentiate lanthanide and actinide complexation properties.[5,7,8]

Various experimental and theoretical investigations have highlighted some differences among chemical bonding properties of trivalent 4f and 5f complexes. Experimentally, systematic comparisons have been carried out mainly on crystallographic studies of isostructural Ln(III) and U(III) complexes and on thermodynamics of complexation in solution.[9−13] These investigations all show that for π-acceptors ligands, the U-ligand bond length is significantly shortened compared to Ln-ligand ones.[9,14−17] This is generally rationalized by the existence of a back-bonding interaction from the U(III) 5f orbitals to the virtual π^* orbital of the π-acidic ligand.[9,12,14,15,17] Infrared stretching frequencies of the π-acceptor ligand (CO, isonitrile) corroborated this effect and showed a decrease compared to the free ligand frequency, as expected for a back-donation interaction.[18]

Nevertheless, it should be stressed that this covalent character is only a weak contribution within a total metal−ligand interaction mostly governed by electrostatic effects. The choice of the theoretical model is thus crucial to probe the bonding nature. For instance, we had previously shown that some DFT methods, namely hybrid functionals including some exact exchange, were unable to reproduce this well-documented back-donation interaction with U(III) and π-acidic ligands.[14−16]

So although it is now accepted that models rooted in DFT may be used to give information on structural and bonding properties[19,20] for heavy element systems, it is still necessary to rely on higher level calculations. Indeed, such f-element complexes combine several difficulties, due to relativity effects and strong electronic correlation, especially static correlation related to the quasi-degenerate valence f orbitals. It is thus desirable to compare the single determinantal solutions obtained within the DFT framework with multiconfigurational approaches. We had already carried out such comparison for trihalide AmX_3 species and shown that a satisfactory reproduction of structural properties could be obtained with DFT, which was comparable to complete active space (CAS) results.[21] Nevertheless in such complexes, f electrons were not involved in the M−X bond, which is mainly ruled by electrostatic interactions. A previous comparative ab initio study has been performed on U(IV), U(V), and U(VI) oxofluorides showing some difference in the geometries and on bonding properties going from DFT/GGA approaches to correlation methods approaches.[22] We thus present here a similar DFT/CAS comparison of methods, but on complexes where the f-electrons are involved in the metal−ligand interaction.

Moreover, the chemical systems were chosen to tune the level of back-donation by varying the oxidation state of U from III to V, which is expected to decrease the back-donation level. The isoelectronic lanthanide species has also been investigated, i.e., the Nd(III) homologue.

Few experimental studies are available for higher oxidation states of U. In a U(V) complex with a bis(diphenyl-diazomethane) ligand, the crystallographic structure[23] showed an elongation of the N−N distance of the ligand, which has been

† Part of the "Vincenzo Aquilanti Festschrift".

* Author to whom correspondence should be addressed. E-mail: valentina.vetere@cea.fr..

‡ Université de Toulouse.

§ Laboratoire de Reconnaissance Ionique et Chimie de Coordination.

|| University of Lund.

⊥ Ecole Nationale Supérieure de Chimie de Paris - Chimie ParisTech.

10.1021/jp904889w
Published on Web 11/05/2009

TABLE 1: Active Space for the Metal and CO Ligand, for F_3UCO, F_3NdCO, F_4UCO, and F_5UCO Species

	active orbitals (active electrons)			
	M^{n+}	CO	active space	spin
F_3UCO, F_3NdCO	7f ($3e^-$)	1σ ($2e^-$), 2π ($2e^-+2e^-$)	9/12	$S = 3/2$
F_4UCO	7f ($2e^-$)	$2\pi^*$	8/12	$S = 1$
F_5UCO	7f ($1e^-$)	$2\pi^*$	7/12	$S = 1/2$

explained by a back-donation mechanism. Instead, experimental studies on a U(IV) complex, i.e., F_4U-CO,[24] do not show such bonding contribution, despite the strong π-acceptor CO ligand. In particular, infrared spectroscopic studies showed on this system a slight increase of the CO stretching frequency (+37 cm^{-1}), compared to free CO. In contrast, the CO stretching frequency when bonded to U(III) strongly decresases (−210 cm^{-1}) compared to free CO,[18] in agreement with a back-donation mechanism from the metal to the π-acceptor ligand.

We have thus carried out a systematic study of the U(III), U(IV), U(V), and Nd(III) bonding properties with the CO ligand, within species of general formula F_nM-CO, with $n = 3$ for U(III) and Nd(III), $n = 4$ for U(IV), and $n = 5$ for U(V). They have been studied by a DFT quasi-relativistic approach on one hand, and by multiconfigurational calculations on the other hand, namely complete active space second-order perturbation theory (CASPT2 approach). All the calculations have been performed using the highest spin states (Hund's rule in the weak ligand field approach) so that U(III) and Nd(III) systems are in a quadruplet spin state, whereas U(IV) is in a triplet state and U(V) in a doublet state. At the DFT level of theory, a complete analysis of the bonding has been carried out in terms of fragments and Kohn−Sham (hereafter KS) orbitals and by the partition of the total energy of the systems in steric and orbital contributions, such analytical tools being present in the Amsterdam density functional code (see Computational Methods).

2. Computational Methods

The CASSCF method, as implemented in the MOLCAS-5[25] quantum chemistry software, has been used. Dynamic correlation has been added to the optimized CAS[26] wave function by a second-order perturbation theory, leading to the so-called CASPT2 method.[27,28] In all the CAS calculations, the active space includes 9 electrons and 12 orbitals for the F_3UCO and F_3NdCO system, 8 electrons et 12 orbitals for F_4UCO, and 7 electrons et 12 orbitals for F_5UCO. Table 1 summarizes the chosen active space and spin state for each species.

Relativistic effects have been introduced by the use of small core relativistic peseudopotentials of Dolg[29] with 32 valence electrons for U (5s5p5d5f6s6p7s). For the lighter elements, F, C, and O, ANO-S (3s2p1d) basis functions have been used.[30]

All the optimized structures at the CASPT2 level have been obtained using grids of points. The presence of symmetry distortions has been checked by breaking the local symmetry. The choice of such grids will be discussed for each system. The geometrical convergence criterion were chosen as 0.001 Å for distances and 0.1 degree for angles.

The DFT calculations have been performed with the ADF99 package,[31] using the LDA functional of Vosko, Wilk, and Nusair[32] combined with exchange gradient corrections of Becke[33] and the Perdew correlation functional.[34] The valence space, described by a Slater type basis set (of triple-ζ quality), includes 6s, 6p, 6d, 5f, 7s, and a 7p polarization orbital for U and 2s, 2p, and a 3d polarization orbital for F, C, and O (triple-ζ basis sets). Core densities have been calculated for each atom by a Dirac−Slater four-component method using the Dirac utility in ADF. The ZORA relativistic Hamiltonian[35] has been used to describe the valence density, in the scalar formalism (BP/ZORA). In all the computations, an unrestricted formalism has been used with spin states as described above.

The convergence criteria were fixed to 10^{-6} hartree and 10^{-5} hartree/Å, respectively for the energy and the gradient and 0.1 degree for angles. The adjustable parameter which controls the precision of integrals and the mesh size for the numerical calculation of integrals, has been augmented to 6.

The orbital visualization has been obtained using the graphical interface CERIUS.[36]

SCHEME 1

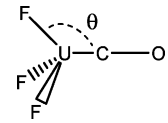

TABLE 2: Optimized Bond Distances (Å) and Pyramidalization Angles θ (deg) for F_3UCO and F_3NdCO Complexes

	method	degrees of freedom	M−C	C−O	U−F	θ
$M = U$	CASPT2	4	2.405	1.160	2.096	112.2
	BP/ZORA	all	2.430	1.150	2.073	113.0
$M = Nd$	CASPT2	4	2.88	1.134	2.12	90.0
	BP/ZORA	all	2.88	1.130	2.08	99.0

3. Results and Discussion

3.1. U(III) Bonding Properties. The general structure of F_3UCO, used for geometry optimization is shown in Scheme 1 and optimized geometrical parameters are collected in Table 2.

For the CASPT2 geometry, a grid of points in C_{3v} symmetry has been chosen; thus, the U−C, C−O, and U−F distances and the pyramidalization angle θ have been optimized, whereas DFT results have been obtained by a full optimization. The two considered theoretical approaches give very close values, in agreement with previous published results.[14] Both the CASPT2 and the DFT geometries show a short U−C distance (about 2.4 Å). The corresponding C−O distance is longer than the one observed for the lanthanide homologues complexes (elongation of around +0.03 Å). More precisely, we should notice that our optimized U−C distances (2.40−2.43 Å) are within the values observed with X-ray structures obtained for two $Cp^{sub}{}_3U-CO$ (Cp^{sub} being a substituted cyclopentadienyl), giving a U−C distance of 2.48 Å or 2.38 Å with $Cp^{sub} = C_5Me_5$ ($Me = CH_3$)[37] or $Cp^{sub} = C_5HMe_4$,[38] respectively.

We have already discussed in previous works that the U(III) bond with a π-acceptor ligand (like CO) is characterized by a back-bonding mechanism that transfers some electron density from the f shells of U(III) to the π^* orbital on the C−O ligand.[14,15] The same trend is here observed by the two ab initio approaches. The KS and CAS-SCF orbitals pictures are really similar (for simplicity we have reported the CAS orbitals picture in Figure 1 and the KS orbitals in the Supporting Information). The analysis of the KS orbitals illustrates well such a back-donation mechanism. The highest occupied orbitals are 2-fold degenerate levels based on occupied 5f orbitals on uranium plus a contribution of ca. 23% of a π^* orbital on the C−O fragment. The third valence f electron is in a pure 5f orbital localized on the U atom.

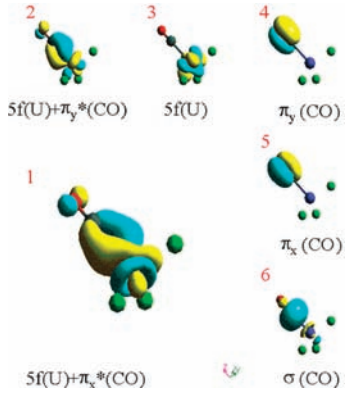

Figure 1. CAS molecular orbitals for UF_3CO. Orbitals 1 and 2 are the singly occupied f orbitals exhibiting a back-bonding mechanism with the π^* orbital on the CO unit. Orbital 3 is the third singly occupied f orbital. Orbitals 4, 5, and 6 are respectively the π_x, π_y, and the σ bonding orbitals of the CO unit.

TABLE 3: Predominant Contributions to the CAS Wave Function for F_3UCO and F_3NdCO Based on the Distribution of the Active Electrons in the Orbital Active Space[a]

F_3UCO

A′				A″		
π	σ	$f_{3-} + f_0$	$f_{1-} + f_{2+} + \pi^*$	π	$f_{1+} + f_{2-} + \pi^*$	weight
2	2	u	u	2	u	0.97

F_3NdCO

A′							A″					
π	σ	f_{3-}	f_{1-}	f_0	f_{2+}	π^*	π	f_{2-}	f_{1+}	f_{3+}	π	weight
2	2	u	0	u	0	0	2	0	0	u	0	0.13
2	2	0	0	u	u	0	2	u	0	0	0	0.57
2	2	0	u	u	0	0	2	0	u	0	0	0.07
2	2	0	u	0	u	0	2	0	0	u	0	0.06
2	2	0	0	0	0	0	2	u	u	u	0	0.06

[a] The "u" means unpaired electron.

The same conclusion can be drawn from the visualization of the CAS orbitals in Figure 1 and from their analysis. The HOMO is constituted by two degenerate orbitals consisting of mixture of the 5f (U) orbitals with π-type orbitals (π_x^*, π_y^*) localized on the CO ligand (orbital numbers 1 and 2 in Figure 1). At lower energy, a pure f orbital contains the third valence electron (orbital number 3 in Figure 1). In Table 3 we report the predominant contributions to the CAS-SCF wave function for the F_3UCO system based on the distribution of the active electrons in the orbital active space. We should notice that although the chosen grid for the optimization uses a C_{3v} symmetry, the CAS wave function is here described in a C_s symmetry scheme. We notice that for such system the CAS wave function is monoconfigurational, so that the DFT single determinant description of U(III) systems is a valid approximation.

Moreover, the harmonic frequency calculation, computed by DFT, shows an important decrease in the CO frequency mode (Table 4) of around 156 cm^{-1}, in agreement with the experimental deviation of around 200 cm^{-1}, from the free CO value to the U bonded CO.[12] Such contraction is consistent with the back-bonding mechanism.

3.2. Comparison of U(III)/Nd(III) Bonding Properties. Optimized geometries for the F_3NdCO complex are collected in Table 2. Both DFT and multiconfigurational approaches give very similar results. The Nd−C bond length is around 0.4 Å longer that the corresponding U(III) one, whereas their ionic radii are similar. This is consistent with a ionic interaction between the Nd(III) and the CO ligand that results in longer equilibrium distances.

TABLE 4: Computed and Experimental Frequencies Modes Corresponding to the C−O Stretching

	DFT/ZORA (cm^{-1})	experimental results (cm^{-1})
ν_{CO} gas	2113	2145
ν_{CO} in F_4UCO	2053	2185
ν_{CO} in F_3UCO	1957	1935

SCHEME 2

Moreover, the analysis of the KS orbitals shows that for the Nd systems, the three highest occupied orbitals are pure 4f orbitals with no interaction with the ligand, so confirming the ionic nature of the bond.

Interestingly, the analysis of the CAS wave function for NdF_3CO shows quite a different behavior from the U(III) homologue. As we can see in Table 3, the Nd complex wave function is strongly multiconfigurational. By permutation of the valence active electrons in the chosen active space, we obtain at least 2 configurations (with weight higher than 0.1) that highly contribute to the ground state description and three other minor contributions with weights that are still higher than 0.05. In contrast, the corresponding U(III) electronic structure shows just one determinant with a weight higher than 0.05.

The difference between the wave function of the two systems can be understood by analyzing the difference between the 4f and 5f orbital due to the ligand fields. The Nd 4f orbitals are almost not split by the ligand field, and they are not mixed with orbitals of different parity (no hybridization), so that they are quasi-degenerate. For such a reason, different electronic configurations are energetically available for electron occupation and give rise to high weight contributions. In the case of U (see Table 3), the 5f orbitals are more diffuse and interact with the ligand orbitals, so that an hybridization phenomenon is observed (to give a better overlap and orientation of the bonding orbital) and the ligand field increases. The configurations obtained by permutation of the valence electrons in the active orbitals are thus nonequivalent, so that one configuration is weight-dominant with respect to the other.

3.3. U(IV) Species: UF_4CO. For the U(IV) complex, the coordination number 5 can lead to two kinds of structure, namely trigonal bipyramid or square pyramid (see Sheme 2, pictures **a** and **b**). Both structures have been studied at the DFT level showing that the bipyramid (structure **a** in Scheme 2) is a much more stable structure (of about 12 kcal/mol). We thus chose the C_{3v} structure (see Scheme 2) as a starting point for a more detailed analysis. In particular, we will call hereafter F_{eq} the three F atoms forming the θ angle with the CO direction, and F_{ax} the F atom on the CO axis.

As above, we decided to study two different structures for the multiconfigurational calculation. In the first one, three parameters were optimized: the U−F distance (i.e., so that $U-F_{ax} = U-F_{eq}$), the U−C and the θ angle, whereas in the second one, we considered a possible axial distortion due to a different $U-F_{ax}$ distance. The BP/ZORA optimizations included the same symmetries as above.

TABLE 5: Distances (Å), Angles θ (deg), and Energy Difference ΔE (kcal/mol) with Respect the Most Stable Geometry at Each Level of Theory (Either CASPT2 or BP/ZORA), for the F_4U-CO Complex[a]

method	free parameters	U−C	C−O	U−F_{ax}	U−F_{eq}	θ	ΔE
CASPT2	3	2.900	1.137		2.080	90.0	2.0
CASPT2	4	2.870	1.138	2.080	2.079	90.0	0
CASPT2	2	2.710	1.140	2.077	2.077	79.9	3.2
SP/CASPT2	0	2.620	1.140	2.056	2.073	79.9	5.0
BP/ZORA	3	2.844	1.147		2.066	90.0	17.3
BP/ZORA	all	2.620	1.140	2.056	2.073	79.9	0

[a] The single point (SP) calculation at the CASPT2 level has been performed on the fully optimized BP/ZORA geometry.

The optimized distances and angles for the U(IV) structure are collected in Table 5. The use of different U−F_{ax} and U−F_{eq} distances does not change much the resulting structures. In contrast, BP/ZORA gives a different description. The first structure, with U−F_{eq} distances equivalent to U−F_{ax} and C−U−F_{ax} angles equal to 90°, is in good agreement with the CASPT2 results. The difference between the two approaches are of the order of 0.02 Å for the U−C distance and 0.01 Å for the U−F ones. Nevertheless, the fully optimized structure at the DFT (BP/ZORA) level shows important differences. First, the pyramidalization angle of the three F_{eq} atoms is important: 80°. Such deformation stabilizes a much shorter U−C bond distance. Moreover, the F_{ax}−U distance decreases. Particular attention should be paid to the fact that the pyramidal structure is now oriented in the direction of the CO ligand, and that they show a longer F−U distance than in the previous structure. Such deformation stabilizes the structure by ca. 18 kcal/mol at the DFT level compared to the constrained optimization. Nevertheless, a single point at the CASPT2 level on such DFT geometry does not stabilize the structure with respect to the previous CASPT2 partially optimized geometries (the energy being around 5 kcal/mol higher than the previous ones).

For the fully optimized DFT structure, frequencies have been checked as being all real. Nevertheless, the frequency corresponding to the C−O stretching mode (2053 cm^{-1}) (see Table 4) do not follow the experimental increase with respect to the free CO stretching frequency.[24] In fact, defining the variation of the CO frequency as $\Delta\nu = \nu(CO)_{bonded} - \nu(CO)_{free}$, we obtain $\Delta\nu = +40$ cm^{-1} for the experimental results and $\Delta\nu = -60$ cm^{-1} for the theoretical one.

The KS population shows important differences. The first DFT structure, with 3 degrees of freedom, shows pure f valence orbitals that do not hybridize with the 6d of the U atom or mix with the CO orbitals. In contrast, the fully optimized one shows a hybridization phenomenon in the valence space, by the mixture of 5f−6d orbitals. A contribution of ca. 5% of the CO orbitals shows a very weak back-donation.

To better understand the distorted structure, we developed a preliminary analysis of the energy partition in term of steric and orbital contributions with respect to the U^{4+}, F^-, and CO fragments. The weak back-bonding interaction stabilizes the structure with an energy gain of around 2 kcal/mol (orbital contribution to the energy stabilization). The highest contribution is electrostatic in nature. In fact, the steric stabilization is divided in two terms: Pauli repulsion and electrostatic interaction (that are computed with respect to the initial fragment electron density). The Pauli repulsion destabilizes the complex with $\theta = 80°$ by ca. 20 kcal/mol, meanwhile the electrostatic gain is higher, of about 35 kcal/mol.

The predominant contributions to the CAS wave function are reported in Table 6, for the F_4UCO system, based on the distribution of the active electrons in the orbital active space. We notice that for such system the CAS wave function is multiconfigurational, so that the DFT single determinant description of U(IV) systems is a poor approximation. The CAS wave function is characterized by a major configuration with 2f electrons distributed in pure f shells, and two secondary configurations (still with non negligible weight with respect to the predominant configuration). In such secondary distributions, we observe in symmetry A″, the presence of one electron in a hybrid f/π* orbital that describes, as we discussed above for the U(III) species, a back-bonding mechanism.

It should be stressed that, despite such f/π* mixture, the U(IV)−CO distance is much higher than the corresponding U(III)−CO one. This can be understood by considering the fact that for the U(III) system just one configuration describes the system and that two electrons occupy the hybrid f/π* orbitals. Meanwhile for the analogue U(IV) system, only secondary configurations involve the unpaired electrons in symmetry A″ into the back-bonding mechanism.

3.4. U(V) Bonding Properties. U(V) is described by a f^1 valence configuration and a doublet ground state. Optimized geometrical parameters at the CASPT2 and DFT BP/ZORA levels of theory are listed in Table 7. Two optimized structures have been obtained from two constrained sets of parameters.

In the first one, the coordination around U is octahedral, with F−U−F angles all fixed at 90° and U−F bond lengths all equal, in a C_{4v} symmetry frame. Thus three free parameters are considered, namely the U−F, U−C, and C−O distances. In the second set of parameters, the U−F_{ax} distance has been optimized independently of the U−F_{eq} one. Both approaches, DFT and CASPT2, give similar results. They all give a ground state wave function of B_2 symmetry. Although the effects of crystal field distortion are usually observed for degenerate ground states, such systems, with a nondegenerate ground state can also exhibit symmetry distortions.

The full optimization was not tractable for the multiconfigurational calculations, but adding one more degree of freedom, with the axial U−F bond being different from the equatorial one, stabilizes the complex by 0.06 kcal/mol.

The CAS predominant contribution to the wave function is reported in Table 8 and shows that the wave function is monoconfigurational. The only unpaired electron is in symmetry B2 and in a pure f shell. No back-bonding mechanism is observed for the U(V) system.

For the BP/ZORA results, we could explore the entire potential energy surface and a new structure has been found with a pyramidalization angle of 82.5° for the four equatorial F with respect to the U-CO axis.

The U−C distance does not change significantly within all these geometrical approaches. This distance, around 2.83 Å, is much longer than that observed for the U(III) complex (2.40 Å for F_3UCO), although the redox state is higher. This is certainly due to two factors: the coordination number is higher for U(V) than for U(III), and the U−CO interaction is ionic for the U(V) system whereas some covalency is observed for the U(III) complex. To describe such ionic interaction, we analyzed the molecular KS orbitals using a fragment analysis in terms of U^{5+}, CO, and F^- initial fragments. This time, the HOMO is a pure f orbital with no orbital contribution coming from the CO ligand.

TABLE 6: Predominant Contributions to the CAS Wave Function for F_4UCO Based on the Distribution of the Active Electrons in the Orbital Active Space[a]

F_4UCO							
A′			A″				
σ	π	$f_{0+} + f_{2+}$	π	$f_{2-} + f_{3-}$	$f_{3-} - f_{2-} + f_{1-} + \pi^*$	$f_{3-} - f_{2-} + f_{1-} - \pi^*$	weight
2	2	u	2	u	0	0	0.69
2	2	u	2	0	0	u	0.18
2	2	u	2	0	u	0	0.09

[a] The "u" means unpaired electron.

TABLE 7: Bond Distances (Å), Angles θ (deg), and Energy Difference ΔE (kcal/mol) with Respect the Most Stable Geometry at Each Level of Theory (Either CASPT2 or BP/ZORA) for the F_5U-CO Complex

method	no. of degrees of freedom	U−C	C−O	$U-F_{ax}$	$U-F_{eq}$	θ	ΔE
CASPT2	3	2.815	1.142		2.062	90	0.06
CASPT2	4	2.836	1.141	2.073	2.061	90	0
BP/ZORA	3	2.837	1.132		2.028	90	0.04
BP/ZORA	all	2.845	1.132	2.049	2.045	82.5	0

TABLE 8: Predominant Contributions to the CAS Wave Function for F_5UCO Based on the Distribution of the Active Electrons in the Orbital Active Space[a]

F_5UCO								
A1	B2			B1			A2	
σ	π	f_0+f_{2+}	π^*	π	$f_{3+}+f_{1+}$	π^*	f_{2-}	weight
2	2	u	0	2	0	0	0	0.96

[a] The "u" means unpaired electron.

4. Conclusion

The comparison of the U(III), U(IV), and U(V) systems shows a strong decrease of the covalent interaction with the increase of the oxidation number. For the U(III) structure, we have no doubt to assess that the shortening of the U−C distance is consistent with the existence of a covalent interaction. We stress that the DFT description of the U(III) bonding with back-donation is fully confirmed by multiconfigurational calculations, consistently with the monodeterminantal nature of the CAS wave function .

While the U(V) species shows a typical ionic bonding, with long U−C distance and valence shells that are pure f noninteracting orbitals, the U(IV) structure does show a very weak back-bonding effect. The variation in the stretching frequency, between free and coordinated CO, is very weak and the analysis of KS orbitals does not show strong participation of the f shells in the bonding. The bonding properties is, in this case, governed mostly by electrostatic interactions.

These trends in the bonding are consistent with the change in U oxidation state from III to IV and V. The partly covalent interaction is specific to the oxidation state III of uranium, which is as expected, much softer than IV and V states. This behavior is quite similar to that commonly observed in d transition metal coordination chemistry, where back-donation is known to occur with low oxidation states. Several examples have shown that the same transition metal bonded to a π-acceptor ligand may give back-bonding or not, depending on the oxidation state; see for instance ref 39. This behavior does not occur with lanthanides, because 4f shells are known to be too contracted to give significant interactions with ligand orbitals. Indeed, the isoelectronic Nd(III) complex gives rise to purely ionic interaction.

Two conclusions may be drawn from this study, related to the modeling and understanding of uranium and lanthanide chemistry. The use of single determinantal methods rooted in the DFT compared to MC approaches seems to give consistent results as far as the description of metal−ligand bonding is concerned. On a more chemical ground, our study enlights the difference between 5f and 4f elements, already well-known in f element chemistry.

Supporting Information Available: KS molecular orbitals for the UF_3CO system. This material is available free of charge via the Internet at http://pubs.acs.org.

References and Notes

(1) Cotton, S. A. *Lanthanide and Actinide Chemistry*; John Wiley & Sons: West Sussex, England, 2006.
(2) Kaltsoyannis, N.; Scott, P. *The f-elements*; Oxford University Press: Oxford, U.K., 1999.
(3) Ansoborlo, E.; Prat, O.; Moisy, P.; Den Auwer, C.; Guilbaud, P.; Carriere, M.; Gouget, B.; Duffield, J.; Doizi, D.; Vercouter, T. *Biochimie* **2006**, *88*, 1605–1618.
(4) Szabo, Z.; Toraishi, T.; Vallet, V.; Grenthe, I. *Coord. Chem. Rev.* **2006**, *250*, 784–815.
(5) Denecke, M. A.; Panak, P. J.; Burdet, F.; Weigl, M.; Geist, A.; Klenze, R.; Mazzanti, M.; Gompper, K. C. R. *Chimie* **2007**, *10*, 872–882.
(6) Mishra, S. *Coord. Chem. Rev.* **2008**, *252*, 1996–2025.
(7) Nash, K. L. *Handbook on the Physic and Chemistry of Rare Earths*; Gschneider, B. V. K. A., Eyring, L., Jr., Choppin, G. R., Lander, G. H., Eds.; Elsevier Science: Amsterdam, 1994; Vol. 18, pp 197−238.
(8) Jensen, M. P.; Bond, A. H. *J. Am. Chem. Soc.* **2002**, *124*, 9870–9877.
(9) Wietzke, R.; Mazzanti, M.; Maldivi, P.; Remy, M.; Latour, J. M. *Inorg. Chem.* **2002**, *41*, 2389–2399.
(10) Brennan, J. G.; Stults, S. D.; Andersen, R. A.; Zalkin, A. *Inorg. Chim. Acta* **1987**, *139*, 201–202.
(11) Adam, R.; Villiers, C.; Ephritikhine, M.; Lance, M.; Nierlich, M.; Vigner, J. *J. Organomet. Chem.* **1993**, *445*, 99–106.
(12) Roussel, P.; Scott, P. *J. Am. Chem. Soc.* **1998**, *120*, 1070–1071.
(13) Iveson, P. B.; Riviere, C.; Guillaneux, D.; Nierlich, M.; Thuery, P.; Ephritikhine, M.; Madic, C. *Chem. Commun.* **2001**, 1512–1513.
(14) Vetere, V.; Adamo, C.; Maldivi, P. *Int. J. Quantum Chem.* **2003**, *91*, 321–327.
(15) Vetere, V.; Maldivi, P.; Adamo, C. *J. Comput. Chem.* **2003**, *24*, 850–858.
(16) Maldivi, P.; Petit, L.; Adamo, C.; Vetere, V. *C. R. Chimie* **2007**, *10*, 888–896.
(17) Kaltsoyannis, N.; Scott, P. *Chem. Commun.* **1998**, 1665–1666.
(18) Brennan, J. G.; Andersen, R. A.; Robbins, J. L. *J. Am. Chem. Soc.* **1986**, *108*, 335–336.
(19) Kaltsoyannis, N. *Chem. Soc. Rev.* **2003**, *32*, 9–16.
(20) Dolg, M.; Stoll, H. *Handbook on the Physic and Chemistry of Rare Earths*; Gschneider, K. A., Eyring, L., Eds; Elsevier: Amsterdam, 1996.
(21) Vetere, V.; Roos, B.; Maldivi, P.; Adamo, C. *Chem. Phys. Lett.* **2004**, *396*, 452–457.

(22) Shamov, G. A.; Schreckenbach, G.; Vo, T. N. *Chem.—Eur. J.* **2007**, *13*, 4932–4947.

(23) Dagani, R. *Chem. Eng. News* **2001**, *8*, 31–32.

(24) Kunze, K. R.; Hauge, R. H.; Hamill, D.; Margrave, J. L. *J. Phys. Chem.* **1976**, *65*, 2026–2027.

(25) Andersson, K.; Barysz, M.; Bernhardsson, A.; Blomberg, M. R.A.; Carissan, Y.; Cooper, D. L.; Cossi, M.; Fleig, T.; Fülscher, M. P.; Gagliardi, L.; de Graaf, C.; Hess, B. A.; Karlström, G.; Lindh, R.; Malmqvist, P.-Å.; Neogrády, P.; Olsen, J.; Roos, B. O.; Schimmelpfennig, B.; Schütz, M.; Seijo, L.; Serrano-Andrés, L.; Siegbahn, P. E. M.; Stålring, J.; Thorsteinsson, T.; Veryazov, V.; Wierzbowska, M.; Widmark, P.-O. *MOLCAS*, version 5.2; Lund University: Sweden, 2001.

(26) Roos, B. O. *European Summerschool in Quantum Chemistry*; Roos, B. O., Widmark, P.-O., Eds.; Universtiy of Lund: Lund, Sweden, 2000; Book II, Chapter VI, p 303.

(27) Roos, B. O. *European Summerschool in Quantum Chemistry*; Roos, B. O., Widmark, P.-O., Eds.; Universtiy of Lund: Lund, Sweden, 2000; Book II, Chapter VI, p 332.

(28) Andersson, K.; Malmqvist, P.-Å.; Roos, B. O. *J. Chem. Phys.* **1992**, *96*, 1218–1226. Andersson, K.; Malmqvist, P.-Å.; Roos, B. O.; Sadlej, A. J.; Wolinski, K. *J. Phys. Chem.* **1990**, *94*, 5483–5488.

(29) Dolg, M.; Stoll, H.; Preuss, H.; Pitzer, R. M. *J. Phys. Chem.* **1993**, *97*, 5852–5859.

(30) Pierloot, K.; Dumez, B.; Widmark, P.-O.; Roos, B. O. *Theor. Chim. Acta* **1995**, *90*, 87–114.

(31) ADF1999.02: Baerends, E. J.; Ellis, D. E.; Ros, P. *Chem. Phys.* **1973**, *2*, 41–51. Versluis, L.; Ziegler, T. *J. Chem. Phys.* **1988**, *88*, 322–328. te Velde, G.; Baerends, E. J. *J. Comput. Phys.* **1992**, *99*, 84–98. Fonseca Guerra, C.; Snijders, J. G.; te Velde, G.; Baerends, E. J. *Theor. Chem. Acc* **1998**, *99*, 391–403.

(32) Vosko, S. H.; Wilk, L.; Nusair, M. *Can. J. Phys.* **1980**, *58*, 1200–1211.

(33) Becke, A. *Phys. Rev. A* **1988**, *38*, 3098–3100.

(34) Perdew, J. P. *Phys. Rev. B* **1986**, *B33*, 8800–8802.

(35) van Lenthe, E.; van Leeuwen, R.; Baerends, E. J.; Snijders, J. G. *Int. J. Quantum Chem.* **1996**, *57*, 281–293.

(36) *Cerius2 Modelling Environment*, Release 4.0; Accelrys Inc.: San Diego, 1999.

(37) Evans, W. J.; Kozimor, S. A.; Nyce, G. W.; Ziller, J. W. *J. Am. Chem. Soc.* **2003**, *125*, 13831–13835.

(38) Parry, J.; Carmona, E.; Coles, S.; Hursthouse, M. *J. Am. Chem. Soc.* **1995**, *117*, 2649–2650.

(39) Gress, M. E.; Creutz, C.; Quicksall, C. O. *Inorg. Chem.* **1981**, *20*, 1522–1528. Shin, Y. K.; Szalda, D. J.; Brunschwig, B. S.; Creutz, C.; Sutin, N. *Inorg. Chem.* **1997**, *36*, 3190–3197. Slep, L. D.; Pollak, S.; Olabe, J. A. *Inorg. Chem.* **1999**, *38*, 4369–4371.

JP904889W